PERGAMON

International Journal of Solids and Structures 39 (2002) 1487–1504

INTERNATIONAL JOURNAL OF SOLIDS and STRUCTURES

www.elsevier.com/locate/ijsolstr

Surface acoustic wave measurements of small fatigue cracks initiated from a surface cavity

Jin-Yeon Kim, Stanislav I. Rokhlin *

Nondestructive Evaluation Program, Edison Joining Technology Center, The Ohio State University, 1248 Arthur E. Adams Drive, Columbus, OH 43221, USA

Received 19 April 2001; received in revised form 14 November 2001

Abstract

A model for the low frequency scattering of a surface acoustic wave by a surface cylindrical cavity with two corner cracks is presented. It is applied to determine the depth of the small fatigue cracks initiated from a pit-type surface flaw. The general scattering formalism based on the elastodynamic reciprocity principle is employed. The effect of the cylindrical cavity on the surface wave reflection from cracks is considered using an approximate stress intensity factor for the corner cracks. In situ surface acoustic wave measurements have been performed during fatigue tests for an Al 2024-T3 sample. The surface wave signal was acquired continuously at different cyclic load levels. The model is verified by comparing calculated reflection signals and spectra with those from experiments. The depths of fully and partially open cracks are determined from the predicted and the measured surface wave reflections. The surface wave reflection is observed to be sensitive to crack closure.

Keywords: Small fatigue crack; Crack closure; Surface acoustic wave; Surface acoustic wave scattering; In situ experiment; Crack depth measurement

1. Introduction

It is important to detect surface flaws and associated cracks and to determine their sizes early in fatigue life in order to prevent catastrophic failure. For the last two decades much effort has been spent on experimental and theoretical investigation of surface wave scattering by surface cracks. Tittman and Buck (1980) performed experiments to measure depth and closure load of surface fatigue cracks in a titanium sample. Khuri-Yakub et al. (1980) and Tien et al. (1981) predicted the size of surface cracks in ceramics using a low frequency scattering model. They studied the effect of the indentation-induced residual stress on crack extension by comparing the results for heat-treated and as-indented samples. Yuce et al. (1985) and Resch and Nelson (1992) performed ultrasonic surface wave measurements to size the depths of small cracks and observed crack closure behaviors for different materials. An experimental study on surface wave interaction with a surface crack has been reported by Yew et al. (1984), in which the crack size was

* Corresponding author. Tel.: +1-614-292-7823; fax: +1-614-292-3395.
E-mail address: rokhlin.2@osu.edu (S.I. Rokhlin).

0020-7683/02/$ - see front matter
PII: S0020-7683(01)00286-4

determined based on the spectrum of the transmitted surface wave. Recently, Rokhlin and Kim (2001) performed ultrasonic surface wave experiments for monitoring surface fatigue crack initiation and growth from a surface flaw and also investigated opening/closure behaviors. Theoretical and numerical studies on the scattering of surface waves by two-dimensional surface breaking cracks can be found in the literature (Mendelsohn et al., 1980; Achenbach et al., 1980; Hirao et al., 1982).

Most of the previous studies are concerned with a crack on a flawless surface. However, fatigue cracks often initiate from surface flaws (e.g., foreign object impact damage, corrosion pit etc.). The additional interaction of the surface wave with the flaw complicates crack detection and prevents immediate application of existing methods to small crack evaluation. The adverse effect of crack closure on nondestructive detection of fatigue cracks is well known. When a fatigue crack is under compressional stress, part of the crack may be tightly closed and the crack may remain undetectable by nondestructive means. On the other hand, the importance of measurement of crack closure stress has been recognized in the area of the fatigue since the actual driving force for crack extension can be estimated from the measurement.

In this paper, a simple model for surface acoustic wave scattering from cracks initiated at the sides of a surface pit is developed. It makes use of a stress intensity factor calculated using an approximate fracture mechanics model for a pit with a corner crack. In situ ultrasonic experiments during fatigue cycling have been performed for Al 2024-T3 alloy samples and the resulting ultrasonic signals interpreted. Pit depths and diameters are determined by analyzing the ultrasonic reflection signals. Calculated time domain reflection signals and spectra are compared with experimental results. The depths of the fully and partially open cracks are determined.

2. Experiment

2.1. Sample and fatigue tests

The material used in the fatigue experiments was a flat sheet of Al 2024-T3 alloy with thickness 1.6 mm. The yield stress (σ_Y) is 340 MPa, the ultimate tensile stress (σ_U) is 483 MPa, and the elongation is 17.5%. The specimens were machined according to ASTM standard E466-96 (1996). Controlled-size small pits with depths of 250–970 μm and diameters of 250 μm were produced by an electrical discharge machine in the center of the surface. Samples having pits with around 250 μm depth were used in the fatigue tests with ultrasonic measurements. Samples with other pit depths were used only for pit depth measurements.

Fatigue tests were carried out on the servo-hydraulic mechanical testing system (MTS) in the load-controlled mode with the following parameters: the frequency of cyclic loading is 15 Hz, the maximum stress level is 76% of the yield stress, stress ratio $R = 0.1$ and the stress range $\Delta\sigma = 231$ MPa. The high stress due to stress concentration leads to the development of a plastic zone around the pit. Considering that the onset of the long crack regime for this material is about 650 μm (Rokhlin et al., 1999), the measurements performed in this study are during and immediately after the short-crack regime of the fatigue life. Post-fracture surfaces were examined with SEM fractographs and actual sizes of crack and pit were measured.

2.2. In situ ultrasonic measurements

In order to monitor crack initiation and propagation during the fatigue cycle, ultrasonic surface wave reflections from the pit and the crack were measured. A commercial wide band longitudinal wave transducer with center frequency 5 MHz was assembled on the specially designed polystyrene wedge and used

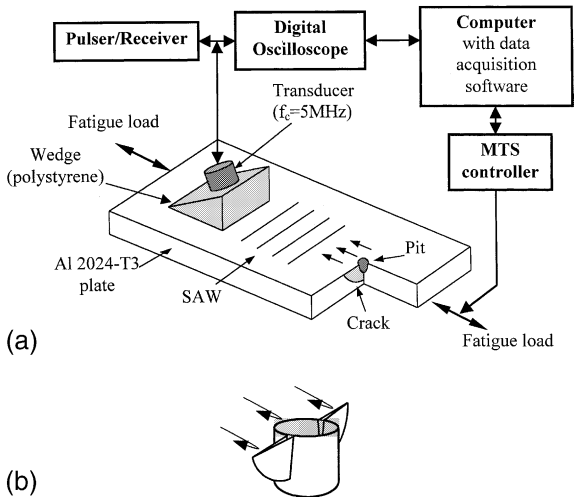

Fig. 1. (a) A schematic illustrating in situ surface acoustic wave monitoring of fatigue crack initiation and growth from a pit. (b) Reflection of surface wave from the pit and the crack surfaces.

for generating and receiving the surface wave signals as shown in Fig. 1. The shape of the wedge was designed to increase the signal-to-noise ratio by eliminating multiple ultrasonic reflections. For an in situ measurement, the transducer assembly is attached on the sample undergoing the fatigue test so that the ultrasonic signals are collected during fatigue cycling and at different load levels. The experimental system includes ultrasonic pulser/receiver, digital oscilloscope, control computer for MTS and ultrasonic data collection. At a predetermined number of cycles, the computer controlled fatigue load was changed to a step-up (10 steps) load (Fig. 2) with recording of ultrasonic reflections at each step-load level. At each load level, the ultrasonic measurements were repeated with a rate of 2 kHz and the reflected signals were averaged in time using the digital oscilloscope to suppress random noise and then fed to the computer in the digital form.

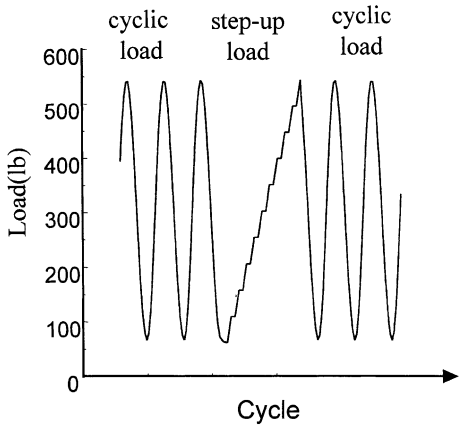

Fig. 2. Load pattern to measure surface wave reflection at different levels of load during fatigue cycle.

3. Ultrasonic results

3.1. Reflection of surface acoustic wave from a pit

A typical reflected ultrasonic signal from a pit is shown in Fig. 3. The surface acoustic wave reflection from a pit is composed of waves reflecting from different corners of the pit, followed by the plate bottom reflections of a mode-converted shear wave. The first group consists of the specular reflection from the front of the pit (1), the creeping wave around the pit (2) and the reflection signal going around the pit bottom and then reflected from the pit opposite corner (3). The amplitude of this reflection signal is much smaller than that of the creeping wave as appears in Fig. 3. The second signal is the plate bottom reflection (4) of the shear wave that is mode converted at the bottom of the pit (and the crack tip when a crack exists). This signal is separated from the pit reflected signals in the time domain. The mode-converted shear wave ((4) in Fig. 3) is launched on the bottom of the pit and propagates down toward the bottom of the plate where it is reflected, mode-converted back to the surface wave at the bottom of the pit, and returned to and received by the surface wave transducer. One can get the depth of the surface discontinuity by analyzing the time delay of the bottom reflection signal.

The frequency spectra of gated signals are shown in Fig. 4. No minimum appears in the spectrum for the signal in gate 1, which implies that there is no signal interfering with the specular reflection in this gate. Note minima in the spectrum of the signal in gate 1 and gate 2 (Fig. 4(b)) due to signal interferences. The

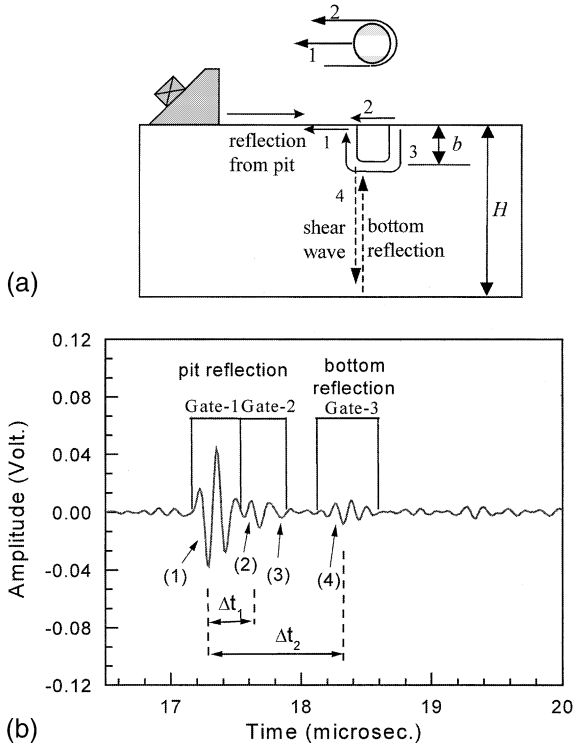

Fig. 3. Back scattering signal of surface wave from a surface pit with 280 μm diameter and 230 μm depth. (a) Different paths of reflected waves; (b) reflections from different corners are marked. The gates for determining time delays are shown. Gate 1 is for the pit front reflection (1); gate 2 is for the creeping wave and corner reflection (2) and (3); gate 3 is for the bottom reflection (4).

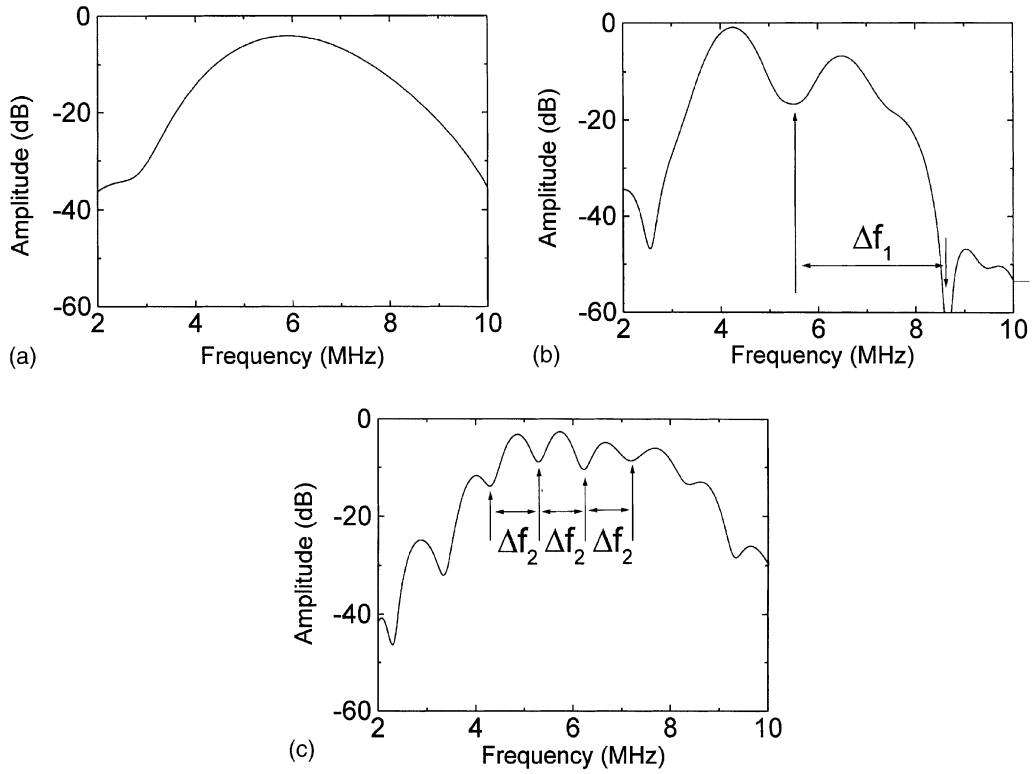

Fig. 4. Spectra of gated signals (Fig. 3). (a) Gate 1 (pit front reflection); (b) gate 1 and gate 2 ($\Delta f_1 = 3.34$ MHz); (c) gate 1 and gate 3 ($\Delta f_2 = 0.98$ MHz).

maximum reflected amplitude from the pit is not affected by the creeping wave since is sufficiently delayed and is smaller in amplitude. In Fig. 5, the signal and its spectrum for the surface wave reflected from a 90° edge are shown. Comparing the spectra in Figs. 4(a) and 5(b), it is found that the spectrum of the pit front reflection (part of the signal in the gate 1) is close to that of the edge reflection signal.

Under the present experimental condition the plate edge can be considered as an ideal quarter space. The surface wave reflection from this edge is not frequency dependent. Therefore, the spectrum shown in Fig. 5(b) can be considered as the incident surface wave spectrum which depends on the transducer and wedge parameters. The reference spectrum of the pulse-echo measurement system $V_i(\omega)$ is determined as a spectral response of the reflection signal from the 90° edge normalized by the theoretical edge reflection coefficient $0.4e^{0.6i}$ obtained from Mendelsohn et al. (1980). This reference spectrum is used to calculate the time domain signals of the surface wave reflection from the cracks.

To interpret the pit reflection signal and to determine the time delay between different contributing components we use the spectrum method. The time delays between the pit front reflection and the surface creeping wave Δt_1 and the pit front reflection and the plate bottom reflection Δt_2 are indicated in Fig. 3. These times can be obtained as inverses of the frequency separations between the spectrum minima (Δf_1 and Δf_2 in Fig. 4). The pit diameter D and depth b are determined from the corresponding signal paths relating the time delays with the pit geometric parameters: $\Delta t_1 = (1 + \pi/2)D/V_R$ and $\Delta t_2 = 2b/V_R + 2(H - b)/V_t$, where H is the sample thickness, V_t is the shear wave velocity and V_R is the Rayleigh surface wave velocity (Fig. 3).

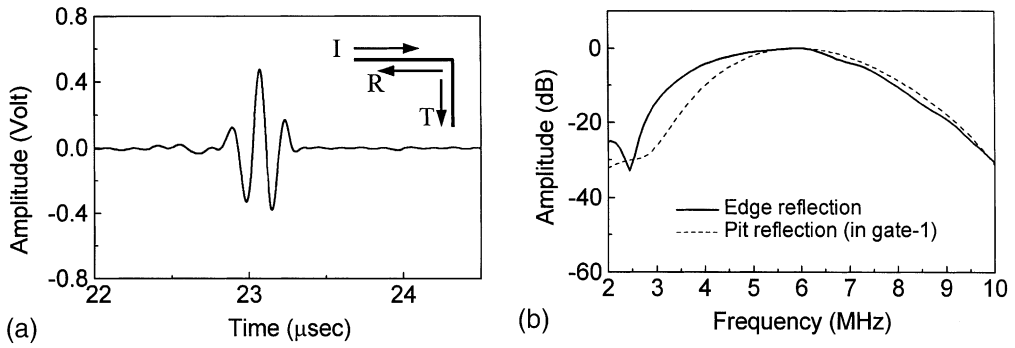

Fig. 5. Time signal (a) and spectrum (b) of surface acoustic wave reflected from 90° edge. The spectrum is compared with that of the pit reflection signal (Fig. 4(a)). Spectra are normalized with maximum amplitudes of signals, $20\log_{10}(S(f)/S_{\max})$.

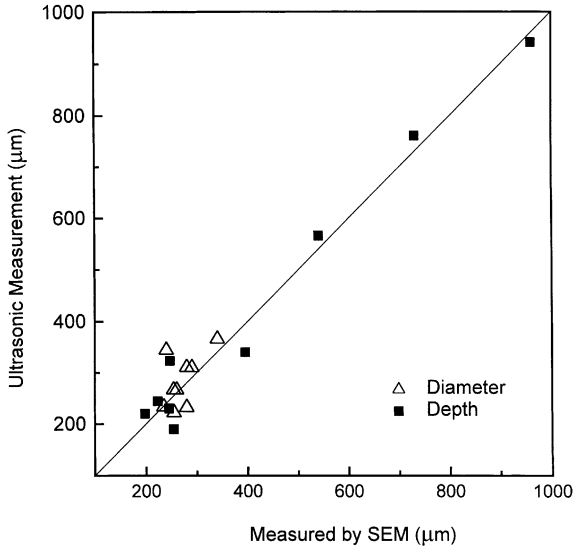

Fig. 6. Comparison of pit dimensions measured from SEM fractographs and calculated from ultrasonic signatures.

In Fig. 6, the pit sizes determined from the spectrum of the reflection signal are compared with those measured from SEM fractographs (Fig. 7) for different pit depths. The result shows reasonable accuracy of the ultrasonic measurements using a 5 MHz transducer for determining the pit size. The discrepancy between the ultrasonic and SEM measurements for shallower pits can be attributed to the fact that the ultrasonic wave detects the pit with a finite width of the beam and thus it provides dimensions averaged over the pit surface.

3.2. Reflection of surface wave from a surface pit with cracks

As an example, Fig. 8 shows surface wave reflection signals acquired at a load level of 191 MPa (400 lbs) and at different numbers of fatigue cycles. As a result of crack initiation and growth from the pit during the fatigue test the amplitudes of both the first ($A^{(1)}$) and plate bottom ($A^{(2)}$) reflections change continuously.

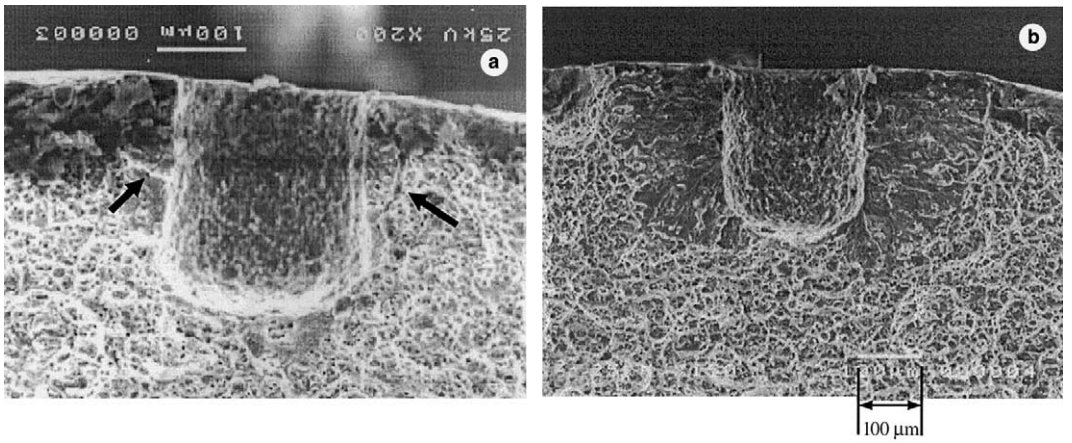

Fig. 7. SEM fractographs of fractured surfaces for measuring actual sizes of pit and cracks. (a) The sample was fractured at 25,000 cycles. Depth and diameter of pit are 256 and 231 μm, respectively. Cracks indicated at the left and right sides of the pit are seen. (b) The sample was fractured at 65,000 cycles. Depth and diameter of pit are 259 and 230 μm, respectively.

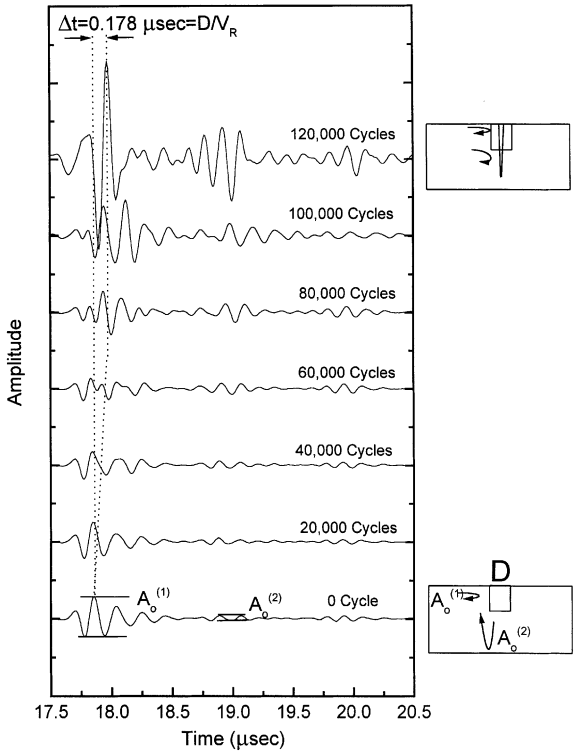

Fig. 8. Surface wave reflection signal from the pit with crack during fatigue cycle. The signal change indicates crack initiation and growth.

Fig. 9 shows peak-to-peak amplitudes of the first and plate bottom reflections from the pit with the crack normalized by those before the fatigue test ($A_0^{(1)}$ and $A_0^{(2)}$ in Fig. 8) at different levels of fatigue load as a

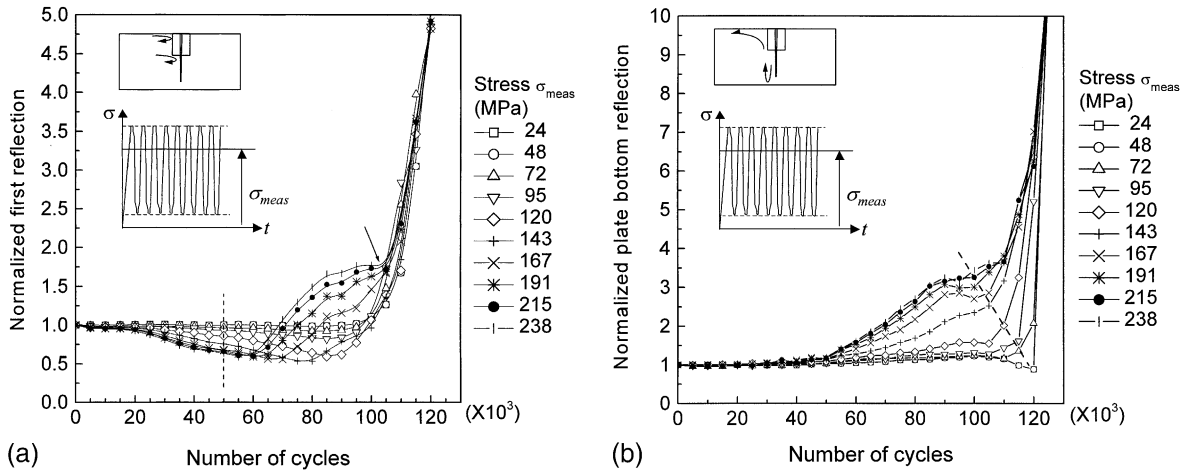

Fig. 9. Change of normalized reflection signal amplitude vs. number of cycles from a pit with crack. Ultrasonic data are taken at different levels of the cycling stresses (as indicated schematically in the figure). The reflection changes due to the crack closure. (a) Normalized first reflection (pit/crack reflection see Fig. 3(b)). (b) Bottom reflection (see Fig. 3(b)). Change of the bottom reflection at 50 k cycles (indicated by arrow) corresponds to the stage of crack growth when it reaches the bottom of the pit.

function of the number of fatigue cycles. Since the crack emanates approximately in the mid-plane of the pit, the path difference (D) of reflected waves from the pit front and crack surface is about half the surface wave wavelength (λ_R) at 5 MHz. Hence, the interference of reflected waves from pit front and crack surfaces becomes destructive. The crack initiation is indicated by the decrease of first reflection amplitude. As the crack grows further, the reflection from the crack eventually dominates the reflection from the pit front and thus the peak amplitude of the first reflection signal shifts by $\Delta t = 0.178$ μs which corresponds to the time for traveling twice the distance of the pit radius (D/V_R) as indicated by the dashed line in Fig. 8 and by the sketch at the right top in the figure.

The amplitude of the plate bottom reflection (Fig. 9(b)) increases monotonically with the number of cycles since it is not affected by wave interference. In Fig. 9(b) at around 50,000 cycles, the second reflection starts to increase with higher slope. The fractograph for the sample fractured at 65,000 cycles after showing the first reflection minimum at 60,000 cycles is shown in Fig. 7(b). The actual crack depth is 265 μm which is slightly more than the pit depth 250 μm. The width of each of the corner cracks is 200 μm. The difference in the number of cycles (60,000 cycles and 50,000 cycles) at which the reflection amplitude has its minimum is due to the distribution of the sample fatigue life. The change of slope happens when the crack becomes deeper than the pit, thus substantially more bottom reflection energy can be captured by the crack surface. Therefore, it can be assumed that the crack depth is near the pit depth at around 50,000 cycles. Thus, the number of cycles at which the plate bottom reflection starts to increase can be used as a reference number of cycles at which the crack depth is the pit depth. The small dips indicated by arrow in Fig. 9(a) and by dashed line in Fig. 9(b) may be attributed to the half wavelength resonance of the surface wave on the crack (Ayter and Auld, 1980). The resonance is weak since the reflection coefficient from the crack tip is small (about 0.2, see Freund, 1971).

As one can see in Figs. 8 and 9, the ultrasonic reflections are sensitive to the load level at which they are measured. This phenomenon is related to the crack opening/closure effect. Details of the ultrasonic determination of crack opening/closure loads can be found elsewhere (Rokhlin and Kim, 2001) and are briefly discussed in Section 5.

4. Low frequency surface wave scattering model

4.1. Scattering theory based on the reciprocity principle

In this section we develop a scattering model to determine the depth of a small crack. The crack size to be considered is up to the depth of the pit (~250 μm). As discussed in Section 2 and reference (Rokhlin et al., 1999), the size of the crack considered in this paper is short in the context of fatigue.

The low frequency scattering theory described by Tien et al. (1981) is extended to consider the pit/crack geometry. The reciprocity relations for the elastic wave scattering from a flaw derived by Kino (1978) and Auld (1979) are applied. Assuming that there is no acoustic source within the volume of interest, the following two states are considered. In state (I) the system is excited by the incident power from a transducer while another transducer receives the response of the system containing the flaw. In state (II) transducers are placed at the same positions as in state (I) but the flaw is absent and the system is excited by the same amount of incident power from the second transducer while the first transducer acts as the receiver. When the second transducer is identical to the first, according to the reciprocity relation (Auld, 1979) the reflection coefficient is given by

$$R_{11}(\omega) = \frac{\mathrm{i}\omega}{4P}\int_S \left(u_i^{(\mathrm{I})}\sigma_{ij}^{(\mathrm{II})} - u_j^{(\mathrm{II})}\sigma_{ij}^{(\mathrm{I})}\right) n_j \,\mathrm{d}S, \tag{1}$$

where ω is the angular frequency, S is the surface of the flaw, $u_i^{(\mathrm{I})}$ and $\sigma_{ij}^{(\mathrm{I})}$ are the displacement and stress fields in state (I), $u_j^{(\mathrm{II})}$ and $\sigma_{ij}^{(\mathrm{II})}$ are those in state (II), n_j means the inward normal vector of the flaw surface and P is the input power to the transmitting transducer. If the internal surface of the flaw is free, that is, $\sigma_{ij}^{(\mathrm{I})} = 0$, Eq. (1) becomes

$$R_{11}(\omega) = \frac{\mathrm{i}\omega}{4P}\int_S u_i^{(\mathrm{I})}\sigma_{ij}^{(\mathrm{II})} n_j \,\mathrm{d}S. \tag{2}$$

Now let us consider corner cracks developed at the two sides of the pit as shown in Fig. 10 and the surface wave normally incident to the crack surface. The reflection coefficient defined above can be separated into two terms: those with integration over the pit surface (S_p) and over the crack surface ($S_\mathrm{c} = S_\mathrm{c}^+ + S_\mathrm{c}^-$)

$$R_{11}(\omega) = \frac{\mathrm{i}\omega}{4P}\int_{S_\mathrm{p}} u_i^{(\mathrm{I})}\sigma_{ij}^{(\mathrm{II})} n_j \,\mathrm{d}S + \frac{\mathrm{i}\omega}{4P}\int_{S_\mathrm{c}} u_i^{(\mathrm{I})}\sigma_{ij}^{(\mathrm{II})} n_j \,\mathrm{d}S = R_{11}^{\mathrm{p}}(\omega) + R_{11}^{\mathrm{c}}(\omega), \tag{3}$$

where S_c^+ and S_c^- are front and back surfaces of the crack. This separation is exact and physically corresponds to the separation of the reflection field into two parts: one mainly from the pit and the second from the crack. It accounts for the phenomenon of interference of reflected waves from the crack and the cavity discussed in Section 3.

Since the stress $\sigma_{ij}^{(\mathrm{II})}$ is continuous across the crack faces, the second integral in Eq. (3) can be expressed as an integral over only the front face:

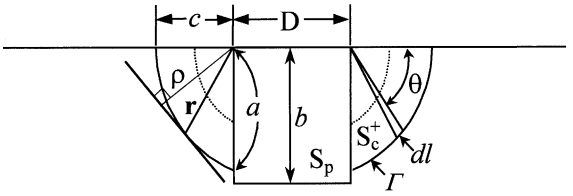

Fig. 10. Geometry of a pit (cylindrical cavity) with corner cracks (see also Fig. 1).

$$R_{11}^{c}(\omega) = \frac{i\omega}{4P}\int_{S_c} u_i^{(I)}\sigma_{ij}^{(II)} n_j \, dS = \frac{i\omega}{4P}\int_{S_c^+} \Delta u_i^{(I)}\sigma_{ij}^{(II)} n_j \, dS, \tag{4}$$

where $\Delta u_i^{(I)}$ is the displacement jump across the crack. Accounting for only the normal stress σ_{zz} of the incident wave, which is dominant at shallow depths, the crack reflection coefficient is approximated as

$$R_{11}^{c}(\omega) = \frac{i\omega}{2P}\int_{S_c^+} \Delta u_z^{(I)}\sigma_{zz}^{(II)} \, dS. \tag{5}$$

Eq. (5) utilizes the symmetric configuration of two corner cracks at both sides of the pit.

Using the results of Budiansky and O'Connell (1976), the crack reflection coefficient can be represented as a contour integral along the crack tip (Γ)

$$R_{11}^{c}(\omega) = \frac{i\omega(1-\nu^2)}{3EP}\int_{\Gamma} \rho(\mathbf{r}) K_I^2 \, dl, \tag{6}$$

where ν is the Poisson's ratio, E is Young's modulus, K_I is the mode I stress intensity factor of the corner crack, $\rho(\mathbf{r})$ is the perpendicular distance from the coordinate origin to the tangential line to the crack tip Γ at the given point $\mathbf{r}$ and dl is the line element on Γ as shown in Fig. 10. Therefore, the reflection coefficient from the crack can be calculated using Eq. (6) if the stress intensity factor for the crack emanating from the pit is known.

The time domain reflection signal is represented using the frequency dependent reflection coefficient in Eq. (5),

$$r(t,a) = \int_{-\infty}^{\infty} [R_{11}^{p}(\omega) + R_{11}^{c}(\omega)] V_i(\omega) e^{i\omega t} \, d\omega, \tag{7}$$

where $V_i(\omega)$ is the frequency characteristic of the measurement system.

4.2. Stress-intensity factor of corner cracks

In our experiments, ultrasonic measurements are performed at $fh = 8$ MHz mm where f is frequency and h sample thickness. At the Rayleigh incident angle both the lowest order symmetric (S_0) and antisymmetric (A_0) Lamb waves [1] are excited with approximately equal amplitudes and phases (see, for example, Viktorov, 1967). Since the stress field of the S_0 mode is symmetrical with respect to the median plane whereas that of the A_0 mode is antisymmetrical, the stresses below the median plane are canceled resulting in a stress distribution very similar to the pure Rayleigh wave (Viktorov, 1967), and the incident stress field can be approximated by that of the pure Rayleigh wave.

To calculate the reflection coefficient R_{11}^{c} in the low frequency approximation the static stress intensity factor due to the stress generated by the incident surface wave is utilized. To obtain the stress intensity factor for this complicated geometry (Fig. 10) we approximate the stress (σ_{zz}) of the incident surface wave as a bending stress in a plate with effective thickness h^* (Tien et al., 1981). Considering that the SAW stress σ_{zz} changes its sign for aluminum at the depth $x/\lambda_R \approx 0.225$ (Viktorov, 1967), we take $h^* = 0.45\lambda_R$ and the bending stress dependence as $\sigma_{zz} = \sigma_0(1 - 2x/h^*)$, where σ_0 is the stress on the surface of the plate. In our experiment the ratio of pit depth b to the effective thickness h^* is $b/h^* \approx 1$. To calculate the stress intensity factor we consider the h^* thick plate with a through-thickness hole as shown in Fig. 11. Using a similar

[1] At low frequencies, S_0 and A_0 modes are the dilatational and the bending vibrations of the plate. At high frequencies (as in our case), both modes approach motion of the surface wave.

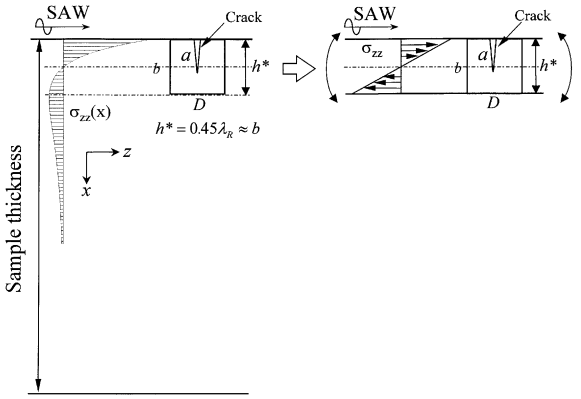

Fig. 11. Effective plate thickness for calculating the stress intensity factor of two corner cracks.

approximation, Rokhlin et al. (1999) analyzed fatigue crack initiation and growth from a pit. They also replaced two cracks at the corners of the pit with equivalent cracks at the corners of the through-thickness hole in a plate with the thickness equal to the pit depth and obtained a good approximation for the fatigue life.

The mode I stress intensity factor for symmetric corner cracks at a through-thickness hole in a plate subject to bending has been calculated numerically by Raju and Newman (1979) and Newman and Raju (1986).

$$K_{\mathrm{I}} = \sigma_0 \sqrt{\frac{\pi a}{Q}} F_{\mathrm{b}}\left(\frac{a}{h^*}, \frac{a}{c}, \frac{D}{h^*}, \theta\right), \tag{8}$$

where a is crack depth, c is surface crack length, D is hole diameter, and Q is a function of the shape factor (a/c) of the crack. The boundary correction factor F_{b} is a function of the crack-and-hole geometries and the angle θ shown in Fig. 10. Raju and Newman (1979) and Newman and Raju (1986) calculated the boundary correction factors for various combinations of geometric parameters. We use their data to calculate interpolated curves for the stress intensity factor of different crack configurations. The interpolated boundary correction factor is shown in Fig. 12(a) as a function of normalized crack depth and in Fig. 12(b) as a function of the angle θ. Note the stress intensity factor is always highest at $\theta = 0°$ for different crack sizes and aspect ratios shown.

To calculate the crack reflection coefficient by means of the stress intensity factor first one should know the shape of the crack. From the SEM pictures of fracture surfaces for samples broken in tension at different fatigue cycles, it is found that the crack aspect ratio (c/a) changes in the range of 0.3–0.8 (Rokhlin et al., 1999) as the crack grows (see Fig. 7).

The reflection coefficient is expressed as the line integral of the boundary correction factor along the front of the two corner cracks,

$$R^{\mathrm{c}}_{11}(\omega) = \frac{\mathrm{i}\omega(1-\nu^2)\pi a \eta_{\mathrm{T}}}{3EQ} \int_C \rho(\mathbf{r}) F^2_{\mathrm{b}}\left(\frac{a}{h^*}, \theta\right) \mathrm{d}l, \tag{9}$$

where $\eta_{\mathrm{T}} = \sigma_0^2/P$ is the factor which is related to the electromechanical efficiency of the transducer (Resch and Nelson, 1992). The line integral is calculated numerically as a function of the crack size with a known boundary correction factor and with the geometric parameters presented above. The normalized crack reflection coefficient $(R^{\mathrm{c}}_{11}(a)/R^{\mathrm{c}}_{11}(b))$ is shown in Fig. 13, where $R^{\mathrm{c}}_{11}(b)$ is the reflection coefficient at the crack

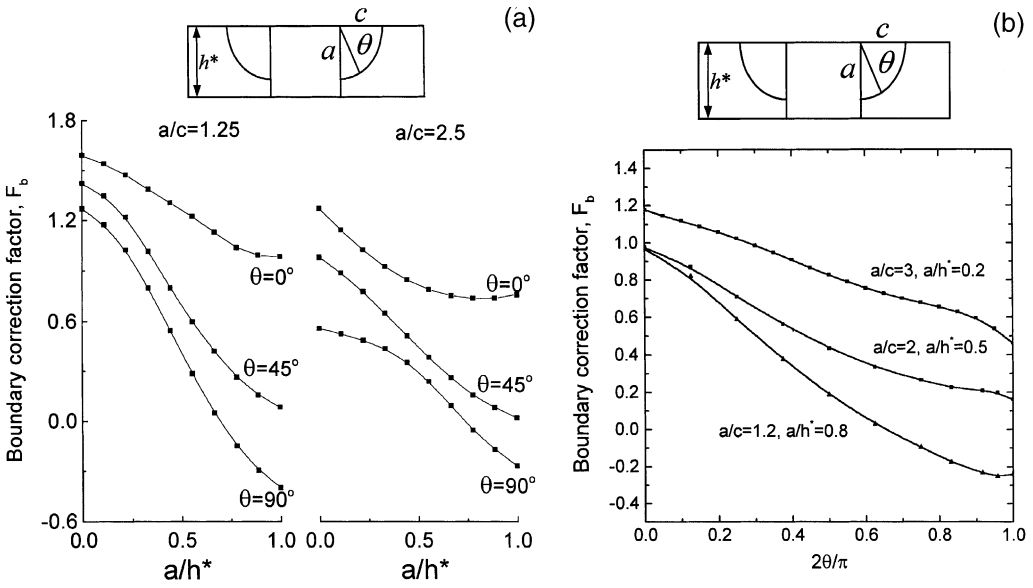

Fig. 12. Boundary correction factor of two corner cracks at both sides of through-thickness hole in a plate under bending load (interpolated and extrapolated from the data in Raju and Newman (1979)): (a) versus crack depth for two aspect ratios; (b) versus angle θ (the curves in this form are used for calculating $R^{c}_{11}(\omega)$ in Eq. (6)).

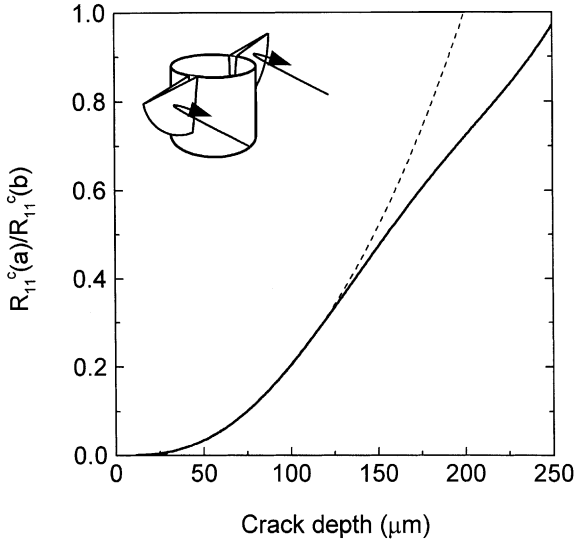

Fig. 13. Reflection from two corner cracks emanating from a cylindrical pit. Normalization is done with reflection from the crack whose depth is equal to the pit depth. Dashed line is the long wavelength approximation ($R^{c}_{11} \sim a^3$).

depth equal to the pit depth ($a = b$). For small cracks, the reflection amplitude depends on the third power of crack depth $R^{c}_{11} \sim a^3$ (dashed line in Fig. 13) which is common to long wavelength scattering (Khuri-Yakub et al., 1980).

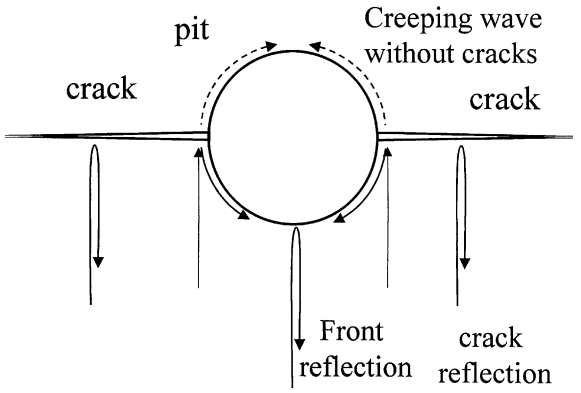

Fig. 14. Creeping wave shielded by cracks.

4.3. Determination of $R_{11}^{p}(\omega)$

The reflection coefficient $R_{11}^{\mathrm{p}}(\omega)$ in Eq. (5) physically corresponds to the wave reflection from the pit front surface and the contribution from the surface wave propagating around the front half of the pit (see Fig. 14). This creeping wave is excited by the surface wave incident at the pit/crack corners. We neglect this creeping wave contribution to the pit reflection coefficient $R_{11}^{\mathrm{p}}(\omega)$ and use the pit front reflection coefficient measured prior to fatigue and thus from the pit without fatigue cracks.

In Section 3.1 we analyzed the effect of the creeping wave on the reflection from a pit without crack. The contribution of pit front reflection and the creeping waves is illustrated by the signals and their spectra in gate 1 and gate 2 in Fig. 3. As one can see from the time domain signals shown in Fig. 8, the cracks shield the creeping wave traveling around the pit diminishing their effect. Thus one can exclude the contribution of creeping waves from the pit reflection, considering only the pit front reflection and represent the time domain pit reflected signal as:

$$\int_{-\infty}^{\infty} R_{11}^{\mathrm{p}}(\omega) V_i(\omega) \mathrm{e}^{\mathrm{i}\omega t}\,\mathrm{d}\omega \approx r(t, a=0), \tag{10}$$

where $R_{11}^{\mathrm{p}}(\omega)$ is the experimental spectrum (Fig. 4a) of the reflection signal in gate 1. The total reflected signal is calculated as

$$r(t,a) = r(t,a=0) + \int_{-\infty}^{\infty} R_{11}^{\mathrm{c}}(\omega) V_i(\omega) \mathrm{e}^{\mathrm{i}\omega(t-D/V_{\mathrm{R}})}\,\mathrm{d}\omega. \tag{11}$$

5. Comparison with experiment and crack size determination

To compare the model prediction with experiment, the time domain signals of the reflected surface wave were calculated using Eq. (11) as a function of the crack depth. The actual crack and pit geometries were determined from SEM fractographs for four samples fractured in tension at the following numbers of fatigue cycles: 25,000, 37,500, 60,000 and 65,000 (Table 1). These measured sizes of the pits and cracks are used for calculating the reflection signals. Figs. 15 and 16 show calculated time domain signals and their spectra for two cases (2 and 3 Table 1) along with the experimental signatures obtained from the same samples. The results are in excellent agreement in both frequency and time domains. A stronger interference

Table 1
Dimensions of pit and crack determined from SEM fractography

Sample #	# of cycles at which sample fractured	Pit		Crack		
		Depth	Diameter	Depth (a)	Surface length (c)	Aspect ratio (c/a)
1	25,000	256	231	123.5[a]	53[a]	0.43
2	37,500	257	253	197	102	0.52
3	60,000	260	262	259	196	0.75
4	65,000	259	230	265	202	0.76

[a] Average values of two cracks.

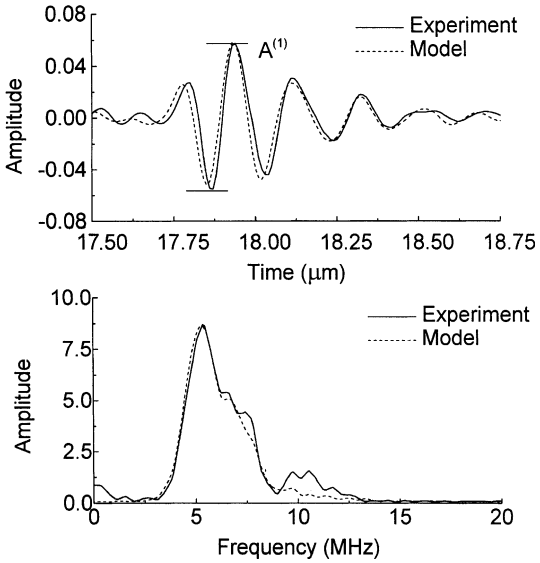

Fig. 15. Comparison of time domain signals and frequency spectra from experiment (a) and model (b). The model calculation was performed using the measured sizes of pit and crack from fractograph at 37,500 cycles: crack depth is determined to be 197 μm; pit depth 257 μm; pit diameter 253 μm.

appears in the time domain signal at 60,000 cycles than at 37,500 cycles, due to stronger reflection from the crack.

Fig. 17 shows the normalized reflection amplitude versus crack depth for different pit diameters (the amplitude determination was done as indicated on the time domain signals in Figs. 15 and 16). At small crack depths the pit diameter significantly affects the dependence of reflected amplitude on crack size: from monotonic decrease to increase of the signal. The range of crack depths calculated in Fig. 17 is up to the pit depth (50,000 cycles as indicated in Fig. 9(a)). To compare with calculations we plotted the measured reflection amplitudes (solid squares) for the samples in Table 1. The results indicate good agreement between calculations and experiment. This illustrates that the present model can be applied for determination of the sizes of cracks emanating from pits if the pit diameter is known. The pit parameters should be determined from ultrasonic measurements prior to crack formation or at minimum fatigue load during the fatigue cycling when the crack is closed. If the crack is open, the pit size can be determined using microradiographic means [Rokhlin et al., 1999] or using the ultrasonic wave technique with application of a compressional stress to close the crack.

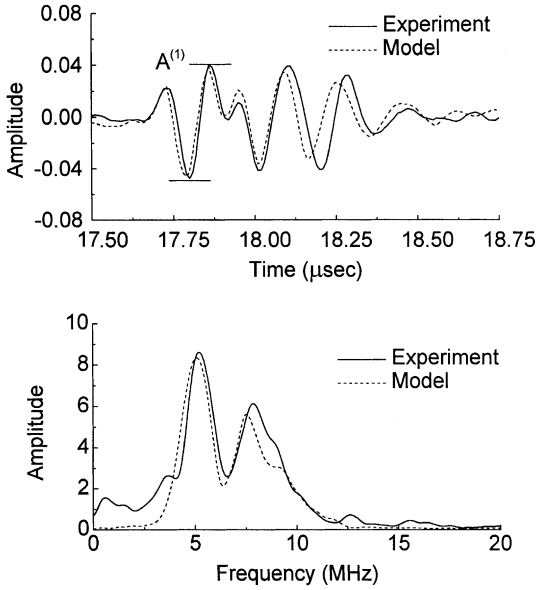

Fig. 16. Comparison of time domain signals and frequency spectra from experiment (a) and model (b). The model calculation was performed using the measured sizes of pit and crack from fractograph at 60,000 cycles: crack depth is determined to be 259 μm; pit depth 262 μm; pit diameter 258 μm.

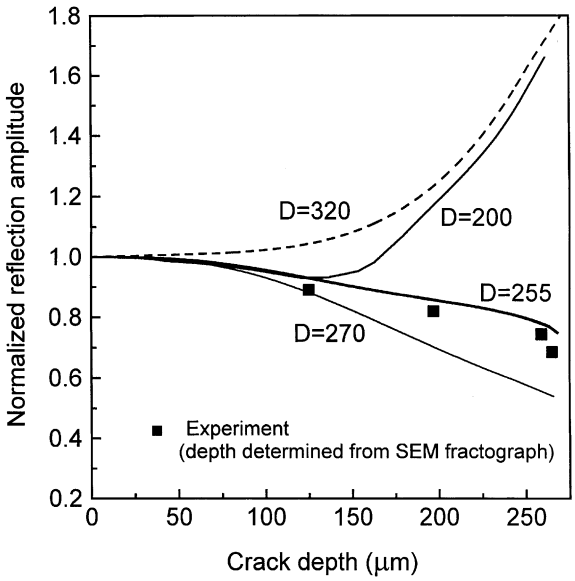

Fig. 17. Normalized reflection amplitude from the corner cracks on the pit for different pit diameters (D). Normalization is performed with the reflection amplitude from the pit prior to fatigue. Solid squares are measurements.

The amplitudes of the first and the bottom reflections are shown in Fig. 9 as functions of the number of cycles at different levels A of the cycling load. At a given number of cycles (crack depth), the reflection amplitude depends on the cycling load level A. This is due to crack closure in the pit plastic zone and the

variation of the length of the open part of the crack (the effective crack length) with load level in the fatigue cycle. A plastic zone is formed around the pit as a result of the stress concentration (k_t) at the pit. To estimate k_t for the pit, the pit is replaced with a hemisphere with a radius equal to the depth of the pit. The stress concentration factor for the hemispherical pit in the plate with finite thickness under equal biaxial stress is $k_b = 2.3$ (Reed and Wilcox, 1970). Using that the stress concentration factor for a through hole is 2 for equal biaxial stress and 3 for tension, the stress concentration factor for a pit in tension is estimated from multiplying k_b by 3/2 to get $k_t = 3.45$. The size of the plastic zone at the fatigue load is estimated to be 250 μm (Rokhlin and Kim, 2001). This plastic zone is constrained by the surrounding elastic medium, thus during the crack growth in the plastic zone compressive closure force is applied to the crack surface. A fresh fatigue crack with perfectly matching surface profiles on the opposite surfaces of the crack under compressive stress becomes perfectly closed, i.e. elastic stresses and displacements are continuous across the crack surface, which is thus absolutely transparent to ultrasonic waves. Under the fatigue cycling it starts to open with load increase. At a given number of fatigue cycles the crack reaches depth a. At the minimum fatigue load, it is completely closed and its effective length is $a_{\text{eff}} = 0$ (Fig. 18). With load increase the crack opens with an increasing a_{eff} (the open part of the crack) and at some stress level becomes completely open, $a_{\text{eff}} = a$. Results shown in Figs. 15 and 16 are related to crack measurements at 238 MPa (500 lb) cycling load at which the crack is fully open.

The depth of the crack at different numbers of cycles can be determined by comparing computed reflection amplitudes versus crack depth ($A^{(1)}$ in Figs. 15 and 16) with experimental reflection signatures obtained at different levels of fatigue load (Fig. 9). In this way, the data in Fig. 17 are mapped into the dependences of effective depths of fully and partially open cracks versus number of cycles (Fig. 19) for a sample at different levels of cycling load showing the dependences of the ultrasonically detectable crack depth (a_{eff}): for example, at around 20,000 fatigue cycles, the actual crack depth determined at the load level 238 MPa (500 lb) is 110 μm whereas the detectable crack depth at the load level 95 MPa (200 lb) is 80 μm. Even though the actual crack depth a reaches the pit depth at 50,000 cycles (see Fig. 9(a)), the effective crack depths at lower load levels can be calculated up to higher numbers of cycles (60,000 cycles in Fig. 19) since the crack depths at the lower loads are still shorter than the pit depth.

Rapid crack growth is observed in the beginning of the fatigue cycle: that is, the crack depth determined at 4600 cycles is already about 70 μm. Thereafter, the crack grows with a lower growth rate until 16,000 cycles, and then with a higher but relatively constant growth rate. This is due to a small crack growth behavior in the residual plastic zone. Due to the high stress concentration at the pit the maximum stress level near the pit is 2.6 times the yield stress. Therefore, the plastic deformation caused by the first half cycle of loading results in compressive residual stresses that retard crack growth (Fig. 19).

The present method allows monitoring the opening/closure behavior of a small fatigue crack (Rokhlin and Kim, 2001); this is difficult to do for small cracks by other methods.

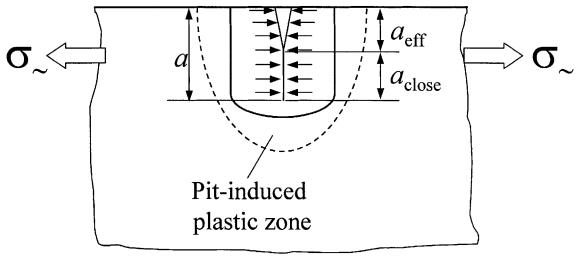

Fig. 18. Schematic of partially closed crack due to compressional stress caused by pit-induced plasticity.

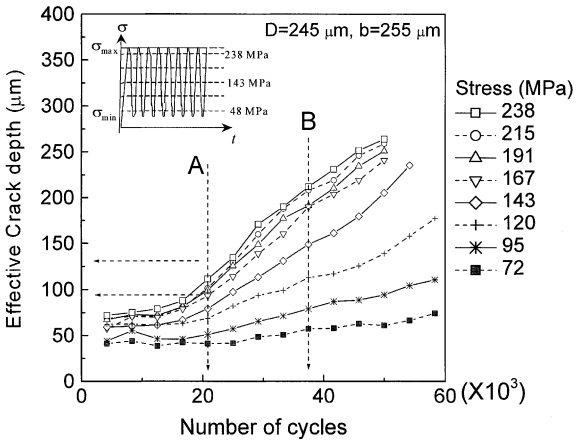

Fig. 19. Effective crack depths calculated from ultrasonic signatures for partially open cracks at different load levels during fatigue cycle.

6. Summary

The ultrasonic monitoring method by means of the surface acoustic wave is developed to characterize small cracks emanating from pit-type surface flaws. Low-frequency scattering theory in conjunction with an approximate fracture mechanics model is developed for calculating the reflection coefficient of two corner cracks on the sides of a cylindrical cavity. In situ surface acoustic wave measurements were performed for Al 2024-T3 samples under fatigue cycling load. Surface wave signals were acquired continuously at different cyclic load levels. The model is verified by comparing with experiment. Using the model the properties of a crack growing in the plastic zone are monitored and depths of fully and partially open cracks are determined during fatigue cycles at different load levels.

Acknowledgements

This work was sponsored in part by the Defense Advanced Projects Agency (DARPA) Multidisciplinary University Research Initiative (MURI) under Air Force Office of Scientific Research grant # F49620-96-1-0442. The authors are thankful to Mr. Dai for his assistance in data collection.

References

Achenbach, J.D., Gautesen, A.K., Mendelsohn, D.A., 1980. Ray analysis of surface-breaking crack interaction with an edge crack. IEEE Trans. Sonics Ultrason. SU-27, 124–129.

ASTM, 1996. Standard practice for conducting force controlled constant amplitude axial fatigue tests of metallic materials (E 466-96). Annual Book of ASTM Standards, vol. 03.01, pp. 466–470.

Auld, B.A., 1979. General electromechanical reciprocity theory relations applied to the calculation of elastic wave scattering coefficients. Wave Motion 1, 3–10.

Ayter, S., Auld, B.A., 1980. On the resonances of surface breaking cracks, Proceedings of the DARPA/AFML Review of Progress in Quantitative NDE, pp. 394–402.

Budiansky, B., O'Connell, R.J., 1976. Elastic Moduli of a cracked solid. Int. J. Solids Struct. 12, 81–97.

Freund, L.B., 1971. The oblique reflection of a Rayleigh wave from a crack tip. Int. J. Solids Struct. 7, 1192–1210.

Hirao, M., Fukuoka, H., Miura, Y., 1982. Scattering of Rayleigh surface waves by edge cracks: numerical simulation and experiment. J. Acoust. Soc. Am. 72, 602–606.

Khuri-Yakub, B.T., Kino, G.S., Evans, A.G., 1980. Acoustic surface wave measurements of surface cracks in ceramics. J. Am. Ceram. Soc. 63 (1,2), 65–71.

Kino, G.S., 1978. The application of reciprocity theory to scattering of acoustic waves by flaws. J. Appl. Phys. 49 (6), 3190–3199.

Mendelsohn, D.A., Achenbach, J.D., Keer, L.M., 1980. Scattering of elastic waves by a surface-breaking crack. Wave Motion 2, 277–292.

Newman Jr., J.C., Raju, I.S., 1986. Stress-intensity equations for cracks in three-dimensional finite bodies subjected to tension and bending loads. In: Atluri, S.N. (Ed.), Computational Methods in the Mechanics of Fracture, vol. 2 (Chapter 9).

Raju, I.S., Newman Jr., J.C., 1979. Stress-intensity factors for two symmetric corner cracks. In: Smith, C.W. (Ed.), Fracture Mechanics-ASTM STP, vol. 677, pp. 411–430.

Reed Jr., R.E., Wilcox, P.R., 1970. Stress concentration due to a hyperboloid cavity in a thin plate, NASA-TN-D-5955.

Resch, M.T., Nelson, D.V., 1992. An ultrasonic method for measurement of size and opening behavior of small fatigue cracks. In: Larsen, J.M., Allison, J.E. (Eds.), Small-crack Test Methods-ASTM STP, vol. 1149, pp. 169–196.

Rokhlin, S.I., Kim, J.-Y., Nagy, H., Zoofan, B., 1999. Effect of pitting corrosion on the fatigue crack initiation and fatigue life. Eng. Fract. Mech. 62, 425–444.

Rokhlin, S.I., Kim, J.-Y., 2001. Ultrasonic monitoring of surface fatigue crack initiation, growth and closure. Int. J. Fatigue, submitted for publication.

Tien, J.J.W., Khuri-Yakub, B.T., Kino, G.S., Marshall, D.B., Evans, A.G., 1981. Surface acoustic wave measurement of surface cracks in ceramics. J. Nondestruct. Eval. 2 (3,4), 219–229.

Tittman, B.R., Buck, O., 1980. Fatigue lifetime prediction with the aid of SAW NDE, In: Proceedings of the DARPA/AFML Review of Progress in Quantitative NDE, pp. 411–421.

Viktorov, I.A., 1967. Rayleigh and Lamb Waves—Physical Theory and Application. Plenum, New York.

Yew, C.H., Chen, K.G., Wang, D.L., 1984. An experimental study of interaction between surface waves and a surface breaking crack. J. Acoust. Soc. Am. 75 (1), 189–196.

Yuce, H.H., Nelson, D.V., Resch, M.T., 1985. The use of surface acoustic waves to study small fatigue cracks in 7075-T651 aluminum and 4340 steel, In: Thompson, D.O., Chimenti, D.E. (Eds.), Review of Progress in Quantitative Nondestructive Evaluation, vol. 4A. Plenum Press, New York, pp. 103–113.